Effects of cohesion on the flow patterns of granular materials in spouted beds

Runru Zhu, Shuiqing Li,* and Qiang Yao
Key Laboratory for Thermal Science and Power Engineering of Ministry of Education, Department of Thermal Engineering, Tsinghua University, Beijing 100084, China

(Received 9 September 2012; revised manuscript received 20 December 2012; published 22 February 2013)

Two-dimensional spouted bed, capable to provide both dilute granular gas and dense granular solid flow patterns in one system, was selected as a prototypical system for studying granular materials. Effects of liquid cohesion on such kind of complex granular patterns were studied using particle image velocimetry. It is seen that the addition of liquid oils by a small fraction of 10^{-3}–10^{-2} causes a remarkable narrowing (about 15%) of the spout area. In the dense annulus, as the liquid fraction increases, the downward particle velocity gradually decreases and approaches a minimum where, at a microscopic grain scale, the liquid bridge reaches spherical regimes with a maximum capillarity. Viscous lubrication effect is observed at a much higher fraction but is really weak with respect to the capillary effect. In the dilute spout, in contrast to the dry grains, the wet grains have a lightly smaller acceleration in the initial 1/3 of the spout, but have a dramatically higher acceleration in the rest of the spout. We attribute the former to the additional work needed to overcome interparticle cohesion during particle entrainment at the spout-annulus interface. Then, using mass and momentum balances, the latter is explained by the relative higher drag force resulting from both higher gas velocities and higher voidages due to spout narrowing in the wet system. The experimental findings will provide useful data for the validation of discrete element simulation of cohesive granular-fluid flows.

DOI: 10.1103/PhysRevE.87.022206 PACS number(s): 45.70.Ht, 45.70.Mg

I. INTRODUCTION

Studies of granular and granular-fluid flows have recently received substantial and renewed attention due to technological needs and also because it is an unsolved problem in fluid physics [1–8]. So far most of the studies have focused on the relatively simple dry granular system with air as the interstitial fluid. In particular, it was reported that the addition of even a small amounts of liquid into a dry granular system can lead to distinct cohesion among the particles [9–11]. On the microscopic grain scale, the role that the pendular liquid bridges strained between two particles has been well studied in the quasistatic regime, with the resulting capillary cohesion being dependent on the liquid surface tension, particle size, contact angle, and liquid volume [12–14]. However, on the macroscopic scale, the interior of the wet granular assembly subsequent to sufficient equilibration is determined by a complex network of nonuniform liquid bridges connecting the adjacent grains in contact. Consequently, not only the detailed connectivity depends on the packing geometry of the granular materials, but each individual liquid bridge also experiences dynamic evolution during the approach or rebound of the particles [11]. So this complex network of capillary bridges under dynamic conditions brings a profound effect to the macroscopic properties of granular assemblies.

The granular assemblies experience remarkably different macroscopic behaviors when exposed to external volume forces (gravity or electric fields), external energy supplies (vibration and shear), and flows of interstitial fluids such as water or air, which may be used to activate the grains. For instance, when the magnitude of these driving forces is sufficiently large, a granular system exhibits transition from granular solid to liquid, in which the various ordered patterns of grains, e.g., resting state, quasistatic dense flow, or rapid granular flow, may develop [4]. Obviously, the effects of the cohesion on each kind of the ordered granular pattern are different. As for the simplest case of a granular pile that is almost at a resting state, the cohesive forces due to liquid bridges increase the static stability of the surface particles of the pile, leading to a dramatically linear increase in the repose angle as a function of the average liquid-layer thickness on the granules [15]. A theory based on the classical Mohr-Coulomb analysis was built to predict the cohesive force and then the pile's maximum angle of static stability, known also as the critical angle (θ_c) [16,17]. As the scaled liquid volume fraction with respect to the total volume of grains, ϕ, successively increases, granular piles experience various kinds of distinct liquid bridge regimes: (1) an *asperity regime* where the cohesive force almost depends on the cube root of the liquid volume, (2) a *roughness regime* where the liquid occupies a statistically rough region with a linear trend between the cohesive force and liquid volume, and (3) a *spherical regime* where the liquid is substantial to ensure that the surface roughness no longer plays a significant role and the cohesive capillary force, insensitive to ϕ, is determined by the macroscopic curvature of the particles. It is further determined that a critical scaled liquid volume ϕ_1 between the asperity and roughness regimes is about 1.4×10^{-4} for glass grains. Below ϕ_1, the granular pile θ_c apparently does not scale with the air-liquid surface tension, whereas it does above ϕ_1 [18]. It is also noted that if ϕ is enough large, in addition to being subjected to attractive capillary forces, moving particles could also be viscously lubricated leading to a *lubricate regime* [12].

In addition to *static* properties, the *dynamic* properties of a wet granular pile also need to be characterized by a partially filled horizontal rotating drum, which is one of the prototypical apparatuses that have been instrumental in the investigation of granular dynamics [2–4,19,20]. Measurements of the angle of maximum stability (θ_m) and the angle of repose (θ_r),

*lishuiqing@tsinghua.edu.cn

 ©2013 American Physical Society

reflecting static and kinetic frictions, respectively, have been made as a function of the volume fraction of the liquid, the grain size, and the dimensions of the wet pile inside the drum [21]. In particular, the granular pattern in the drum is divided into two regions: a rigidly rotating bulk pile and a surface granular flow that is only a few layers deep. As the rotation rate increases and decreases, the surface flow has been observed to exhibit hysteretic transition from a stick-slip avalanche regime ($\theta_m > \theta_r$) to a continuous avalanche regime ($\theta_m \approx \theta_r$) [22,23]. The effects of the cohesion on this avalanche-continuous flow transition are quite complicated, consisting of three flow regimes of the surface layer: *granular*, *correlated*, and *viscoplastic*. For a lower ϕ at a magnitude close to the asperity regime of bridges ($\sim 10^{-4}$), the behavior of the surface layer is qualitatively similar to the dry case with a distinct hysteretic transition, which is termed a granular regime. At a relatively large ϕ with either roughness regime or spherical regime of liquid bridges, the correlated regime of granular assembly occurs as the grains stick together due to the considerable cohesive force and form clumps in the surface layer, eliminating the hysteresis of the transition. If the ϕ is extremely large, the lubrication effect results in a viscoplastic regime of granular surface flow where the transition occurs at relatively low rotation rates with a reappearing hysteresis.

In order to attain a general understanding of the role of cohesion in granular materials, the configurations reported here can provide more distinct and complex granular patterns, which need to be explored. More recently, two-phase granular-fluid systems, in which large amounts of interstitial air agitate the gains and significantly complicate the dynamics of granular materials, have received renewed attention [4,7,8,24–26]. Here a two-dimensional spouted bed (2DSB), which is a special fluidization technology for handing Geldart-D coarse particles, is selected as an example because it offers a number of important features. First, the flow patterns of granular materials in spouted beds are nearly periodic and can attain a quasisteady state over a long operational time [27,28]. That is, similar to the rotating drums, spouted beds also possess two distinct ordered granular patterns but are much more complex, i.e., a core of upward dilute granular-fluid flow called the "spout" and a surrounding region of downward dense quasistatic granular flow called the "annulus." In the spout the grains experience the gas drag and inelastic collision, while in the annulus the densely packed grains slowly move under gravity and friction similar to a hopper flow. It is thus of interest to understand how the cohesion affects these two distinct granular-fluid patterns, either dilute or dense, in one bed. However, so far the literature on this subject is inconceivably scarce [29]. A research methodology can be referred to previously systematic studies on rotating drums [18–22,30]: not only the geometry dividing different flow regions, but also the detailed velocity profiles should be determined to characterize the dynamics properties. Second, the system is relatively simple as compared to multiorifice fluidized beds since it has only one nozzle for the agitation of grains, and as such can be easily scaled and modeled. Third, besides its importance from the basic scientific perspective, spouted beds have a valuable contribution in industrial applications such as drying, coating, granulation, combustion, coal gasification, and chemical vapor deposition [31–33].

In this paper, we aim to clarify the roles of the cohesion in both dense and dilute flow patterns of granular materials in a two-dimensional spouted bed. Section II describes the experimental setup and procedure. In Sec. III we first measure the velocity profiles of the granular particles in the dilute "spout" and dense "annulus" regions by a modified Particle Image Velocimetry (PIV) technique developed in our laboratory. Then, the influence of cohesion on the spout-annulus interface is investigated. Furthermore, the effects of cohesion on the granular velocities in the densely packed annulus are discussed. We try to extrapolate the dynamic macroscopic granular behaviors to the microscopic regimes of liquid bridges between two particles. Finally, effects of cohesion on the granular acceleration in the dilute spout are determined and then explained by a mathematical model based on gas-solid mass and momentum balance.

II. EXPERIMENTAL SETUP

The apparatus, 2DSB, consists of a vertical rectangular column with cross-sectional dimensions of $L_x = 15.2$ cm and $L_z = 1.5$ cm and is connected to a lower wedge-segment base with an inclined angle of 60°and height $H_c = 11.52$ cm. The experimental procedure and measurement are similar to our previous work for studying dry granular-fluid flows [28]. Initially, the bed is filled with spherical glass beads of diameter $d_p = 2.5$ mm and density $\rho_p = 2380$ kg/m^3. For all cases, the total mass of the glass grains in the bed is about 86.1 g, keeping a 7.0 cm static height existing in the wedged section, as shown in Fig. 1. Air is introduced from an inlet nozzle

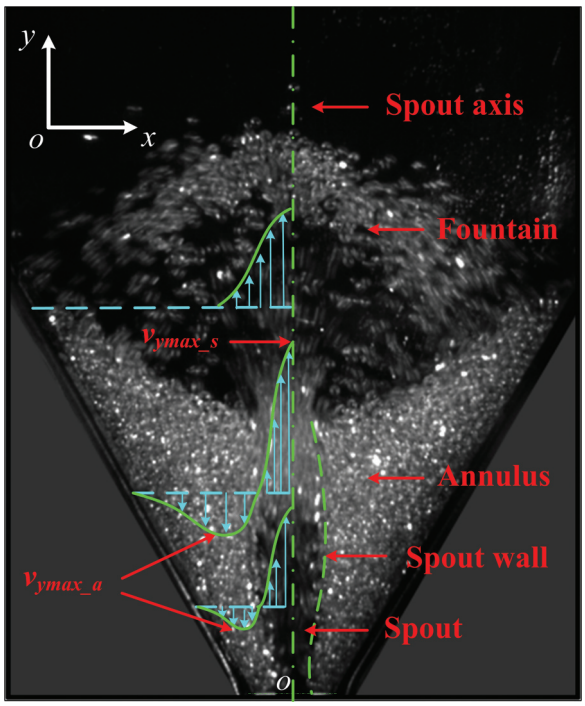

FIG. 1. (Color online) Image of grain behaviors in 2DSB; the schematic of vertical particle velocity files in distinct regions (blue arrows) and spout wall (green dashed line). $v_{y\max\_s}$ and $v_{y\max\_a}$ are the maximum vertical particle velocities in the spout and the annulus, respectively.

($L_{\text{in}} = 0.9$ cm width), located at the lowest position of the wedge segment, to agitate the granular pile. The superficial velocity U_g with respect to the cross section of 15.2×1.5 cm is about 1.08 m/s. When regular spouting is achieved, a certain amount of the nonvolatile polydimethylsiloxane (PDMS) oil is injected over the top of the granular bed. The surface tension Γ and the viscosity η_l of the PDMS oil are 0.021 N/m and 9.35×10^{-3} kg $(\text{m}^{-1}\,\text{s}^{-1})$, respectively. The amount of added liquid volume is scaled to a fraction ϕ, defined as the ratio of the liquid volume to the physical volume of all beads. As mentioned above, the asperity regime of the liquid bridge ($\phi \sim 10^{-4}$) does not affect the macroscopic granular flows. In this experiment, ϕ varies from 2.76 to 16.5×10^{-3}, which covers both the *roughness* regime and the *spherical* regime of the liquid bridges [17].

To ensure that the bed operates at a "two-dimensional" instead of a "slot-rectangular" mode, the ratio $L_z/L_x = 1.5/15.2$ adopted is considered to be small enough to eliminate significant third-dimensional effects (i.e., the particle mixing along the thickness L_z [28,34,35]). Meanwhile, to reduce wall friction effects, the ratio of thickness L_z to particle diameter should be large enough. In this work, the ratio of $L_z/d_p = 6.0$ exceeds the critical value of 5.0 reported in the literature [19,28].

The images of the granular materials are taken from one end of 2DSB by using a high-speed camera (IMperX, IPX-VGA210-G). The glass front plate permits optical access, whereas the back stainless steel surface is anodized black to minimize optical noise effects. The camera provides the resolution of 228×330 pixels at 700 frames per second and can continuously record for several seconds. The flow area is illuminated by two identical 500 W fluorescent lights symmetrically placed beside the bed. The particle velocity profiles for the entire bed are extracted using an internally developed PIV algorithm such that the distinct flow pattern can be quantitatively characterized. The details of the PIV technique for granular flows were described in detail in our recent work [27,28]. Briefly, the direct normalized cross-correlation algorithm for two sequences of images is used to calculate the velocity fields of particles. In each case, we had averaged 1000 sequences to obtain the time-averaged velocity fields of the 2DSB with maintaining a good repeatability. As shown in Fig. 1, the image snapshot clearly shows that 2DSB has a clear geometrical boundary of three regions: the dilute central spout, the extended fountain, and the dense annulus regions. From PIV measurements, it was previously reported that the lateral profile of the particle vertical velocity (v_y) in the spout is a nearly third-polynomial function with a maximum value, $v_{y\,\max\_s}$, at the spout axis [28]. At the annulus-spout interface (namely, the half spout-wall width r_s), the particles entering the spout from the annulus imply a gradient-free condition of $\partial v_y/\partial x|_{x=r_s} = 0$ or $\partial v_y/\partial x|_{x=r_s} > 0$. It means the particle velocity profile in the spout has an inflection point, which enables the mean velocity of the lateral profiles to be equal to the half of the maximum velocity. In the annulus, with increasing lateral distance from the spout wall, the particle vertical velocity increases very fast to a maximum $v_{y\,\max\_a}$ and then slowly decreases in a quasilinear fashion as it approaches the wedge wall. The magnitudes between $v_{y\,\max\_a}$ and $v_{y\,\max\_s}$ differ by at least one order.

III. RESULS AND DISCUSSION

Aiming to elucidate roles of the liquid cohesion in the granular flow patterns of 2DSB, the results are presented in the following sequence. Direct visualization of the flow patterns of both dry and wet granular materials is first conducted, which is followed by a discussion of the effect of cohesion on the geometrical boundary dividing the distinct granular patterns. The velocity profiles of dry or wet particles in these granular patterns, e.g., both the dilute spout and the dense annulus regions, are quantitatively characterized and theoretically explained.

A. Distinct granular patterns in 2DSB

Despite the known classification of the spout, annulus and fountain regions of spouted beds, there has been little discussion on the related granular patterns. Referring to Fig. 1, the pattern of grains in the spout behaves like granular gases but with bilateral inelastic collisions in such a narrow zone. We have observed, even for dry grains without cohesion, that they move as collective clusters instead of individual particles. As the cluster moves upward, it collects particles from the annulus and progressively grows larger and denser. The spout wall is not steady; it instead is coherent with a frequency of 7.7 Hz [28]. The inherent dissipation due to the inelastic collisions could be one reason for the clustering [5,36]. Consequently, the grains in the fountain next to the spout become more dispersed and ballistic because of the dramatically increased flow area while still behaving as granular gases. As the grains freely fall back to the annulus region, the granular pattern behaves as a slow gravity-driven, dense flow similar to that of a hopper flow, being affected by both inelastic collision and friction.

In order to assess the effect of liquid cohesion on the above granular patterns and since the liquid oil is introduced at the upper surface of the spout, it is crucial to determine the time to achieve a uniform distribution of the liquid. Figure 2 shows

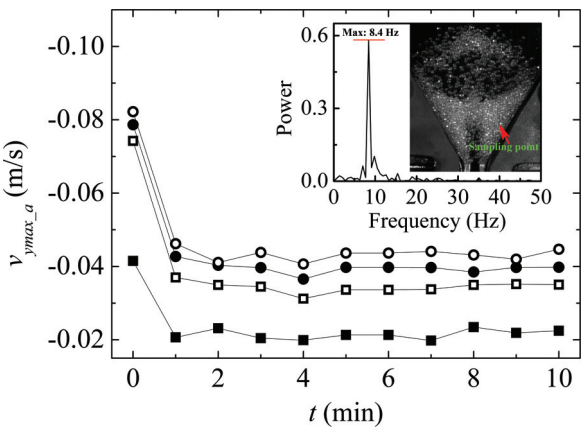

FIG. 2. (Color online) Variation of the maximum vertical velocity of particle, $v_{y\,\max\_a}$, in the annulus with time. Under the scaled liquid volume fraction $\phi = 2.76 \times 10^{-3}$, for various bed levels of $y =$ 0.45 cm (closed squares), $y = 1.13$ cm (open squares), $y = 1.58$ cm (closed circles), and $y = 2.03$ cm (open circles). Inset to this figure shows the PSD distribution corresponding to the fluctuation of vertical particle velocity, v_y, at a sampling point ($x = 2.1$ cm, $y = 4.35$ cm). The dominant frequency was 8.4 Hz.

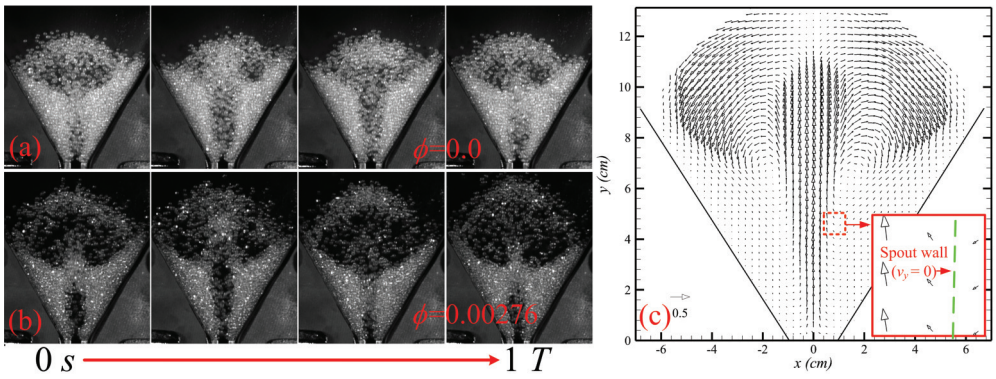

FIG. 3. (Color online) (a) Flow patterns for $U_g = 1.08$ m/s for dry granular system; (b) flow patterns for $U_g = 1.08$ m/s for wet granular system ($\phi = 2.76 \times 10^{-3}$); (c) the time-averaged velocity profile of wet granular system ($\phi = 2.76 \times 10^{-3}$).

the variation of $v_{y\,\max\_a}$ with time, where $v_{y\,\max\_a}$ is the time-averaged maximum vertical velocity of particles at various bed levels of the annulus. It is seen that, for all bed levels y, in just 1 minute the values of $v_{y\,\max\_a}$ under the dry condition are dramatically reduced to almost half (50%) of their values under the wet condition. Subsequently, from 1 to 10 minutes, changes of the annulus particle velocity are quite small, and as such can be characterized as a quasisteady period. It was reported that the periodicity of incoherent spouting in 2DSB could result in the periodic motion of annulus particles in terms of an acceleration → deceleration → stagnation process by the same frequency. The inset of Fig. 2 shows the power spectral density (PSD) distribution for the instantaneous v_y at a sampling point ($x = 2.1$ cm, $y = 4.35$ cm) under the wet $\phi = 2.76 \times 10^{-3}$ condition exhibiting a frequency of 8.4 Hz ($T = 0.12$ s), which is slightly faster than to the 7.7 Hz ($T = 0.13$ s) of the dry case. This then implies that there are about 500 recirculation cycles of the grains in the spout even in 1 minute, enabling the attainment of an equilibrium state of the liquids with grains, as shown in Fig. 2.

Figure 3(a)–3(b) shows the photographic sequences of flows patterns within one cycle T for both dry and wet granular systems, with a superficial velocity of $U_g = 1.08$ m/s. It is seen that the cohesion under $\phi = 2.76 \times 10^{-3}$ causes a narrower spout region (i.e., spout-annulus interface) and a higher fountain region. The time-averaged particle velocity vector fields, shown in Fig. 3(c), were obtained from PIV results over more than 10 cycles of periodicity (∼1000 sequences). The inset figure shows that the half width of the spout wall (r_s) can be determined from the position where v_y vanishes.

B. Effect of cohesion on the spout geometry

Although the liquid volume fraction ϕ is as small to 2.76×10^{-3}, it has a dramatic effect on the spout-annulus interface that classifies the observed distinct granular patterns. As shown in Fig. 4(a), the total height of the spout region is about 6 cm, and then the spout width of wet grains along the spout axis is smaller than that of the dry one. The inset indicates the ratio of the wet spout width ($\phi = 2.76 \times 10^{-3}$) to the dry one. It starts with a value of 0.73, rapidly increases

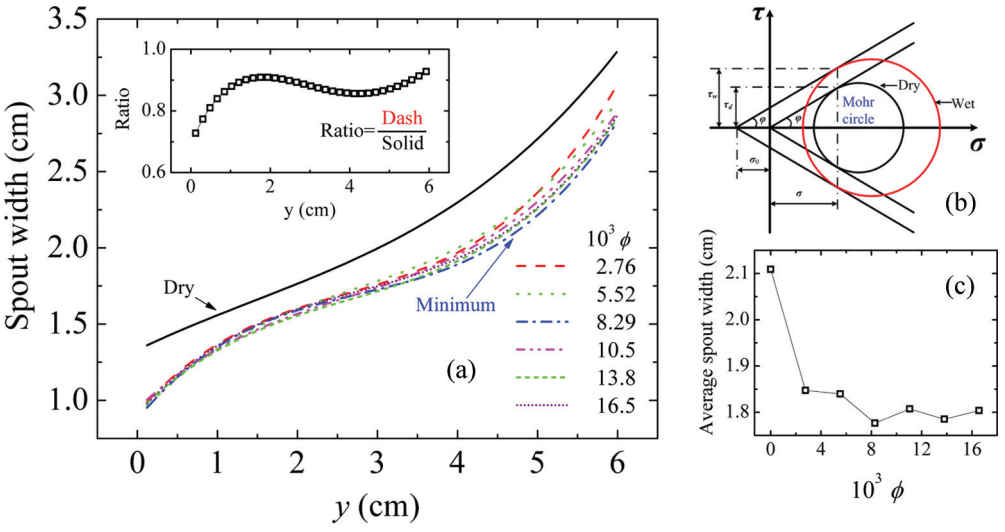

FIG. 4. (Color online) (a) Variation of the width of spout wall along the axis for different liquid volume fractions ϕ. Black line indicates the data for dry system. Upper inset shows the ratio of the spout width between dry and wet granular system at $\phi = 2.76 \times 10^{-3}$. (b) The Mohr circle stress diagrams for dry (black circle) and wet (red circle) granular systems. (c) Variation of the mean spout width for cases with different ϕ.

to 0.91 within 2 cm, which is 1/3 of the spout zone [termed stage I in Fig. 7(a)], and finally maintains a small fluctuation from 2 to 6 cm [termed stage II in Fig. 7(a)]. As we increase ϕ by almost a factor of six, from 2.76×10^{-3} to 16.5×10^{-3}, the spout width in stage I almost does not change. However, in stage II, the spout width slightly decreases and reaches a minimum (blue dash dot line) at $\phi = 8.29 \times 10^{-3}$, followed by a much smaller increase with further increase in ϕ. Figure 4(c) further shows the average spout width of 2DSB, $\bar{x}_s = 2\bar{r}_s$. It is seen that the value of $\bar{x}_s$ for dry case is 2.11 cm, whereas those of the six different wet cases slightly range from 1.78 to 1.85 cm, implying that the flow area of the wet cases occupies about 84.2%–87.6% of that of the dry case.

It then behooves us to ask as why does cohesion cause such a large difference. According to the principle of least action, in order to maintain the regular spouting, the work done to create the spout cavity, namely, the work of the external forces trying to prevent its formation, is the minimum work needed to avert the collapse of the annular bed. Thus, the kinetic energy of the inlet air should overcome not only the normal stress (σ) due to the gravity of the bed materials, but also the shear stress (τ) at the spout-annulus interface. As for the granular materials, the Coulomb yield criterion takes the form $\tau = \sigma \tan\varphi + c$, where φ is the internal friction angle and c is the coefficient of cohesion. As shown in the Mohr circle of Fig. 4(b), the shear stress force, with respect to the normal stress, for wet grains (red circle) is much larger than that for dry grains (black circle). An approximate relationship between the shear stress at the interface of the spout annulus and the lateral gas pressure gradient was proposed as $\tau = (r_i/2)dP/dx$ [37,38], where r_i is half-width of inlet nozzle for both wet and dry cases. Therefore, it requires a smaller spout width to accommodate a larger shear stress, for the same total kinetic energy provided by the inlet air.

C. Effect of cohesion on granular velocities in a dense annulus

We now examine the effects of cohesion on the annulus granular pattern. Figure 5(a) shows the lateral profiles of the vertical particle velocity in the annulus for different ϕ at a bed level of $y = 5.08$ cm. The negative value indicates that the granular flows are directed downward. As ϕ increases from 0 to 5.52×10^{-3}, except at two vicinities close to the spout wall and wedge wall, the flow of wet grains becomes slower. However, as ϕ exceeds 8.29×10^{-3}, the changes in the particle velocity profiles as a function of ϕ are not appreciable. For a quantitative comparison, we select the maximum $v_{y\,\max\_a}$ of all lateral profiles at $y = 2.03$, 3.50, 5.08, and 5.88 cm and plot the variation of $v_{y\,\max\_a}$ against ϕ in Fig. 5(b). The value of $v_{y\,\max\_a}$ decreases as the bed level goes down. At each bed level, as ϕ increases from 2.76×10^{-3} to 10.5×10^{-3}, $v_{y\,\max\_a}$ keep a slightly successive decrement. The position of $\phi = 10.5 \times 10^{-3}$ can be regarded as a critical point for the data at all bed levels. Below it, the effect of cohesion on the annulus granular flow is continuously enhanced, which could be attributed to the increasing cohesive force from the roughness regime to the spherical regime of the liquid bridges. Above it, the effect almost keeps constant or even becomes worse. It implies the lubrication effect to the capillary cohesion at relatively higher ϕ.

In order to relate the macroscopic granular flow properties to the microscale liquid bridges between discrete grains, we define V as the amount of liquid present per particle contact, and we obtain $V \propto \phi$. The roughness of glass grains can be characterized by a mean radial length scale l_R for the fluctuating fragments and the lateral distance scale l_d between the two fragments. For the glass grains used here, we used the roughness length scales, $l_R \approx 1$ μm and $l_d \approx 5$ μm from the literature [18,39]. The experiments here involve both the roughness and spherical regimes of the liquid bridges, with ϕ_2 as a boundary point. In the spherical regimes ($\phi \geqslant \phi_2$ or $V \geqslant V_2$), the capillary cohesive force between two particles is expressed as

$$F_c = 2\pi R\Gamma \cos\theta, \tag{1}$$

where R is the particle radius, Γ the surface tension of the liquids, and θ is the contact angle between the liquid and the grain surface. In the roughness regimes ($\phi_1 < \phi < \phi_2$ or $V_1 < V < V_2$), the cohesive force is linear in the volume of the liquid bridges, $F_c \propto \Gamma V \propto \Gamma\phi$. Noting that $V_1 = l_R l_d^2$ and $V_2 = l_R^2 R$ [17,18], the cohesive force in the roughness regime can be approximately as

$$F_c = 2\pi R\Gamma \cos\theta \frac{V}{V_2}. \tag{2}$$

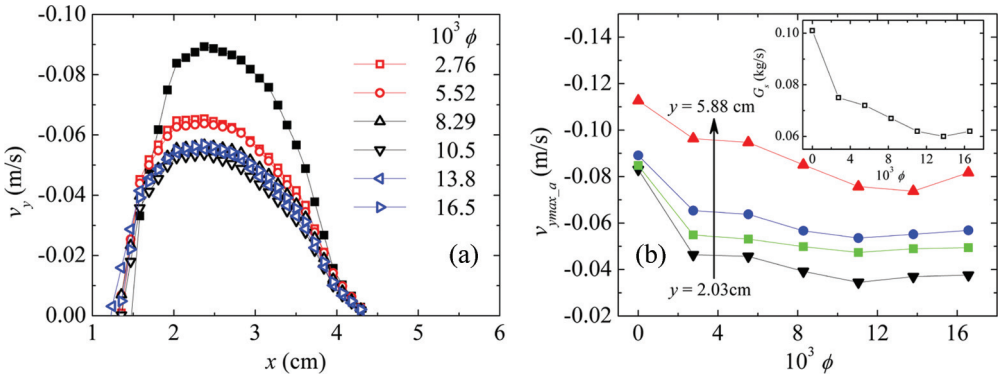

FIG. 5. (Color online) (a) Lateral profiles of the vertical particle velocity in the annulus for different ϕ at a bed level of $y = 5.08$ cm. Solid squares denote the corresponding data for dry system. (b) Variation of $v_{y\,\max\_a}$ with ϕ for various bed levels. Bed levels range from 2.03 to 5.88 cm. Inset shows the particle circulation rate G_s under different ϕ.

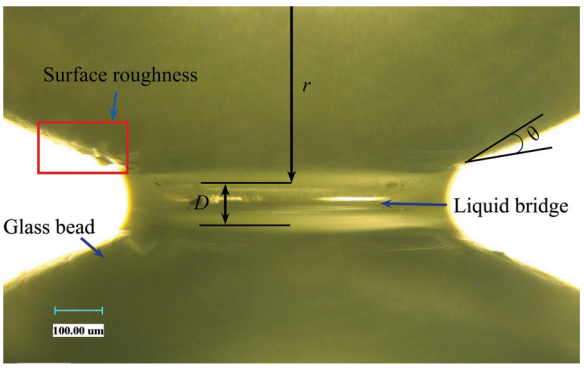

FIG. 6. (Color online) Microscope image for liquid content $\phi = 0.0165$. Liquid bridges between the glass beads are clearly visible. θ is the contact angle, D is the distance between two particles, and r is the radius of the grain.

Since the first critical volume $\phi_{1,}$, which is the boundary between the asperity and roughness regimes, has a magnitude of 10^{-4}, we obtain ϕ_2 as

$$\frac{\phi_2}{\phi_1} = \frac{V_2}{V_1} = \frac{l_R R}{l_d^2} \approx 100. \tag{3}$$

Consequently ϕ_2 has a magnitude of 10^{-2}, which remarkably coincides with the critical $\phi = 10.5 \times 10^{-3}$ for classifying granular flow regimes in Fig. 5. As the liquid bridge overcomes the roughness regime and reaches the spherical regime maintaining a maximum capillary cohesion, the continuing addition of liquids eventually leads to the appreciable viscous lubrication. For instance, the slight reincrement of the particle downward velocity at $\phi = 16.5 \times 10^{-3}$ demonstrates existence of the viscous effect to cohesion.

By experimentally sampling the particles, the liquid bridge of the two representative particles is clearly shown in Fig. 6.We define a separation distance D as the gap between the spherical surfaces of two bridging particles. Here D is about 80–100 μm, which is much larger than both l_R and l_d. However, in the dynamic granular flow system, the separation D varies during contact duration of the two particles [1,12]. In fact, during approach, Eq. (1) is extended to describe the dynamic capillary force between the two particles as

$$F_c = 2\pi R\Gamma(\cos\theta)X_V, \tag{4}$$

while the viscous (lubrication) force is given as [1,12]

$$F_v = \frac{3}{2}\pi R^2 \eta_l \frac{1}{D}\frac{dD}{dt}X_V^2, \tag{5}$$

where η_l is the liquid viscosity, dD/dt the approaching velocity between the two particles, and X_V, the approaching factor, expressed as $X_V = 1 - [1 + 2V/(\pi R D^2)]^{-0.5}$. By assuming a constant volume of all bridges in the granular assembly, the V per particle contact can be approximately estimated by ϕ as [40]

$$V = \frac{8\pi R^3 \phi}{3(1-\varepsilon_a)N}, \tag{6}$$

where N is the coordination number of the bridges around a particle and ε_a the voidage of the annulus. Assuming a nearly constant annulus voidage, the voidage of the cohesive granular assembly in the densely packed annulus is given as [41]

$$\frac{\varepsilon_a - \varepsilon_0}{\varepsilon_{\max} - \varepsilon_0} = \left(\frac{\phi}{\phi_{\rm cr}}\right)^{0.423}\left[1 - 0.421\ln\left(\frac{\phi}{\phi_{\rm cr}}\right)\right], \tag{7}$$

where ε_0 is the packing voidage of the dry granular assembly, and ϕ and $\phi_{\rm cr}$ are the real and critical liquid volume scaled by the granular volume. Note that in Ref. [41], the scaled liquid mass with respect to the granular mass, M, instead of ϕ, is adopted. They have a linear relationship given by $M = \phi\rho_l/\rho_p$.The critical $\phi_{\rm cr}$, resulting in the highest $\varepsilon_{\max}$, is empirically given as

$$\phi_{\rm cr} = 0.2545\left(\frac{\rho_l}{\rho_p}\right)^{-2.057}{\rm Bo}^{-0.4743}, \tag{8}$$

where the particle Bond number, ${\rm Bo} = \rho_p g d_p^2/\Gamma$, is a measure of the surface tension force compared to the body force. Then we obtain $\varepsilon_{\max} = \varepsilon_0 + 0.048{\rm Bo}^{-0.423}$ at $\phi_{\rm cr}$ [41]. In this work, we know that $\theta = 10.0^{\rm o}$, $\varepsilon_0 = 0.42$, $N = 6.0$, $\rho_l = 935$ kg/m^3, $\rho_p = 2380$ kg/m^3, and $g = 9.8$ m/s^2. Then, for $\phi = 16.5 \times 10^{-3}$ in Fig. 5, we estimate the voidage ε_a to be 0.431, and then V as 7.91×10^{-11} m^3. We define the maximum separation distance, where the amount of liquids cannot bridge the two spheres anymore, as the rupture distance $D_{\rm rup}$, which can be precisely predicted by Ref. [14]

$$D_{\rm rup} = (1 + \theta/2)V^{1/3}. \tag{9}$$

Consequently, we obtain $D_{\rm rup} = 467$ μm, which is reasonably larger than the value of 80–100 μm of the equilibrium separation of bridging particles sampled from the granular bed, as shown in Fig. 6. In order to further evaluate the viscous effect, we define a lubrication number as the ratio between the viscous and capillary forces in Eq. (4) and (5):

$$\mathscr{L} = \frac{F_v}{F_c} = \frac{3}{4}\frac{R}{D}\frac{dD}{dt}\frac{\eta_l}{\Gamma}\frac{X_V}{\cos\theta}. \tag{10}$$

The approach velocity dD/dt has the magnitude of 0.01 m/s from Fig. 5. As D varies at 50, 100, and 250 μm, the corresponding $\mathscr{L}$ is estimated as 6.33%, 2.31%, and 0.37%. According to the observed liquid bridge in Fig. 6, there exists a relatively weak lubrication effect at a high ϕ, which causes a slight reincrement of the particle downward flow, in contrast to the dramatic reduction due to the capillary cohesion.

The solid circulation rate, G_s, defined as the integral of the products of the particle mass flux $(\rho_p(1-\varepsilon_a)v_x)$ and interface area along the bed length, can be expressed as $G_s = \int[\rho_p(1-\varepsilon_a)v_{x,i}](2L_z)\,dy$, where $v_{x,i}$ is the lateral velocity of the particles at the annulus-spout interface directing from the annulus to the spout, ε_a the annulus voidage defined in Eq. (7) with the ignorable changes, and L_z the thickness of the bed. As shown in the inset of Fig. 5(b), with increment of ϕ, G_s gradually decreases and nearly approaches its capillary-driven asymptotic limit at $\phi = 10.5 \times 10^{-3}$. The small reincrement of G_s at $\phi = 16.5 \times 10^{-3}$ also confirms the weak lubrication effect.

D. Effect of cohesion on granular velocities in dilute spout or fountain

Figure 7 shows the longitudinal profile of the vertical particle velocity (v_y) along the spout axis under different ϕ.

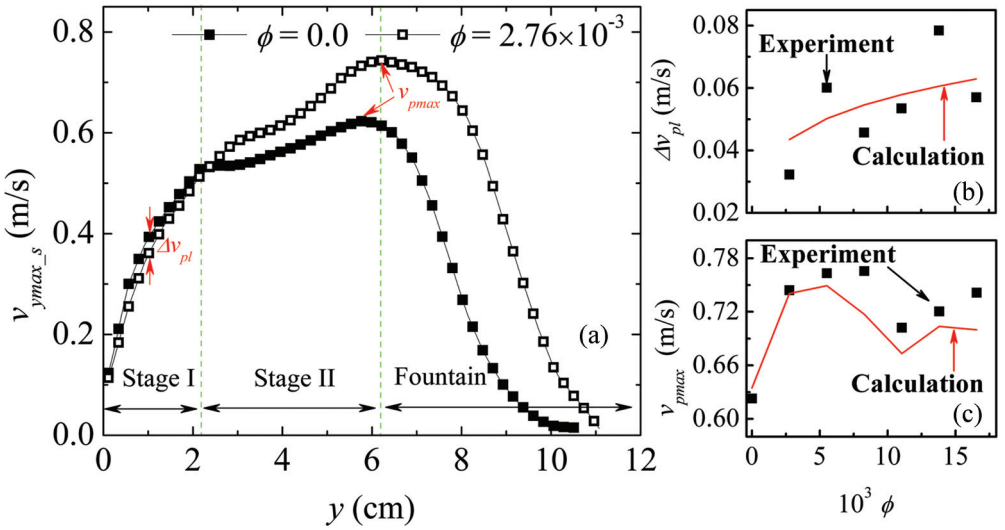

FIG. 7. (Color online) (a) The longitudinal profile of vertical particle velocity along the spout axis. Δv_{pl} represents the particle velocity difference between cases $\phi = 0.0$ and $\phi = 2.76 \times 10^{-3}$ at bed level $y = 1.02$ cm. (b) The Δv_{pl} in stage I, for both experiments and theoretical predictions, under different ϕ. (c) The maximum vertical particle velocities $v_{p\max}$ in the spout, for both dry and wet systems, under different ϕ.

It is seen that, for both dry and wet systems, the dilute spout or fountain region can be considered to consist of three zones, namely, a rapid acceleration stage (stage I) from zero to 2.0 cm height, a slow acceleration stage (stage II) reaching the top of the spout at nearly 6.0 cm, and a deceleration stage known as fountain (stage III). The grains in stage III behave as classical free projectile motions as they acquire enough inertia from the spout. Considering the two acceleration stages of the spout, it is then of interest to note that while the wet grains possess slightly smaller v_y than the dry grains in stage I, they become dramatically larger in stage II, hence indicating the complexity of the effects of cohesion.

Stage I close to the orifice is highly diluted as seen from the photos of Fig. 3. The flow pattern can be described as a free jet to entrain the particles from the annulus and then to accelerate them individually. For the cohesive particle, the kinetic energy, transferred from gas to an individual particle at the annulus-spout interface, is also used to overcome the interparticle cohesive energy in addition to dragging it. As mentioned above, the viscous force is very small in contrast to the capillary force. Thus, the cohesive energy needed to separate two particles is approximately the integration of the capillary force over the contact-to-rupture distance:

$$W_c = \int_0^{D_{\rm rup}} F_c dD. \tag{11}$$

Close to the annulus-spout interface, the particle velocities are quite small. Assuming the kinetic energy of wet grain at rupture distance approaches null, the dry grain possesses a large kinetic energy that equals W_c. Thus, the particle velocity difference, Δv_{pl}, between the dry and wet grains at the rupture time is determined by employing $W_c = \pi d_p^3 \rho_p (\Delta v_{pl})^2/12$. Then this Δv_{pl} is roughly conserved in the stage I because of the nearly same acceleration for both dry and wet grains. As shown in Fig. 7(b), for different ϕ, the predicted Δv_{pl} from Eq. (11) agrees well with the velocity difference measured between the dry and wet systems. This weak dependence can be explained as below. W_c is proportional to $D_{\rm rup}$ and then depends on liquid volume by the power 1/3. So a relation of $\Delta v_{pl} \propto \phi^{1/6}$ exists.

In stage II of the spout, using the mass and momentum balance equations, we can explain why the wet grains have a relatively larger vertical particle velocity as compared to the dry ones, as shown in Fig. 4. First, from mass conservation of the solid phase, we obtain

$$\rho_p x_s \frac{d\left[(1-\varepsilon_s)\, v_s\right]}{dy} = \frac{dG_s}{dy} = 2 v_{x,i}\,(1-\varepsilon_a)\,\rho_p. \tag{12}$$

The annulus voidage ε_a is in a narrow range of 0.42–0.44 according to Eq. (7), the spout width is given in Fig. 4(a), and $v_{x,i}$ is determined from PIV measurements, e.g., in Fig. 3(b). It is noted that v_s represents the mean vertical velocity of particles in the spout. In recent work for dry grains, we discovered that the lateral profiles of vertical particle velocity, v_y, at all bed levels of the spout almost behave cubically with the maximum values, $v_{y\max\_s}$, occurring at the spout axis [28]. We normalize v_y by $v_{y\max\_s}$ at the spout axis and x by r_s, and then draw lateral profiles at $y = 5.88$ cm for both dry and wet cases into Fig. 8. It is found that wet grains still obey the nearly cubical function between $v_y/v_{y\max\_s}$ and x/r_s. The fact that this third-degree polynomial profile has an inflection point ensure a relationship, $v_s \approx v_{y\max\_s}/2 = v_y(x=0)/2$. Figure 7(a) shows the values of $v_{y\max\_s}$ along the spout axis. Thus, the spout voidages along the bed axis, predicted by Eq. (12), are illustrated in Fig. 9(a). In stage I, the voidages between the dry and wet grains are very close. However, in stage II, the wet grains possess higher voidage than the dry grains, with a difference of about 0.04–0.05 at the upper spout end. This can be considered as one of the reasons for the more rapid acceleration of the wet grains in stage II shown in Fig. 7(a).

To proceed further, we need the information of gas velocity and pressure drop in the spout. Using the gas-phase momentum

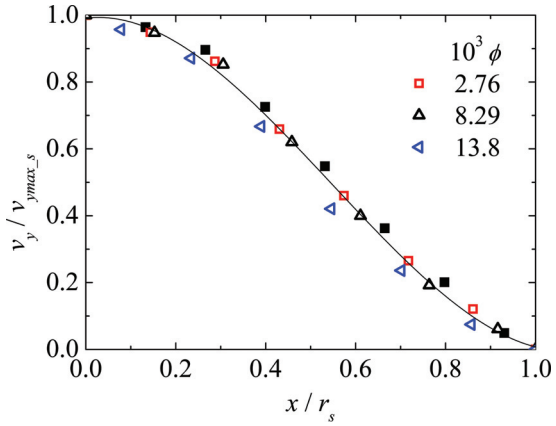

FIG. 8. (Color online) Lateral profiles of the scaled particle velocity, $v_y/v_{y\max\_s}$, in the spout as a function of the scaled x/r_s at a bed level of $y = 5.88$ mm. Dry grains: solid square symbol; wet grains: open symbols for various $\phi = 2.76$, 8.29, and 13.8×10^{-3}.

conservation of the spout, we obtain

$$\rho_f \frac{d\left(\varepsilon_s u_s^2\right)}{dy} = -\varepsilon_s \frac{dp}{dy} + \beta\left(v_s - u_s\right), \tag{13}$$

where u_s is the mean y-component velocity of the gas fluids in the spout, and β the drag force coefficient and expressed by a combination of the Ergun and Wen-Yu equation as

$$\beta = \begin{cases} \frac{\eta_f(1-\varepsilon_s)}{d_p^2 \varepsilon_s}\left[150\left(1-\varepsilon_s\right) + 1.75\mathrm{Re}_p\right] & \varepsilon \leqslant 0.8 \\ \frac{3}{4} C_D \frac{\eta_f(1-\varepsilon_s)}{d_p^2} \varepsilon_s^{-2.65} \mathrm{Re}_p & \varepsilon > 0.8. \end{cases} \tag{14}$$

In the above the drag coefficient C_D for a single particle, is evaluated as

$$C_D = \begin{cases} 24\left(1 + 0.15\mathrm{Re}_p^{0.687}\right)/\mathrm{Re}_p & \mathrm{Re}_p \leqslant 1000 \\ 0.44 & \mathrm{Re}_p > 1000. \end{cases} \tag{15}$$

$$\mathrm{Re}_p = \frac{\left|u_s - v_s\right| \rho_f \varepsilon_s d_p}{\eta_f}, \tag{16}$$

where η_f is the gas viscosity and Re_p the particle Reynolds number. The integral form for the mass conservation of the gas phases is given as

$$U_a A_a = Q_0 - \varepsilon_s u_s A_s, \tag{17}$$

where Q_0 is the total volumetric flow rate of the inlet gas, U_a the superficial gas velocity in the annulus, A_s ($= x_s \times L_z$) and A_a ($= (x_c - x_s) \times L_z$) the cross-sectional area of the spout and the annulus, respectively, and x_c is the width of the wedge section of 2DSB, for which the pressure drop in the spout is almost equal to that in the annulus. And the pressure drop in the annulus depends on the viscous resistance due to the small velocity. Consequently, we obtain

$$\frac{dp}{dy} \approx \left(\frac{dp}{dy}\right)_a = -150\frac{(1-\varepsilon_a)^2}{\varepsilon_a^3}\frac{\eta_f}{d_p^2} U_a. \tag{18}$$

Substituting Eq. (17) into (18) and then finally into (13), u_s is numerically solved for the known v_s and ε_s. To facilitate convergence of the solution, we set the initial pressured drop by using the empirical Lefroy-Davidson expression [42,43]. Figure 9(b) shows the predicted u_s at different bed levels, with the inset indicating the pressure drop. It is seen that the value of u_s in each wet system is much higher than that in the dry system, whereas the pressure drop is much lower. By estimating the flux at the end of the upper spout, it is found that, in the dry case, about 35.7% of the total fluid percolates into the annulus from the spout, which agrees well with the data reported on conical spouted beds [44,45]. Then, under wet cases at $\phi = 2.76 \times 10^{-3}$ and 16.5×10^{-3}, the gas fraction percolating into the annulus is slightly reduced to 32.1% and 29.9%, respectively. Therefore, for the 2D geometry, distributions of the gas flows between the spout and annulus are insensitive to either the liquid cohesion or the spout diameter, but depend on the packing characteristics in the annulus. Since dry and wet cases both have relatively close voidages in the annulus, percolation of the gas across the spout-annulus interface should be similar. The similar gas distributions, together with the reduced spout widths in the wet cases, cause higher u_s, lower U_a, and then lower pressure drops, as shown in Fig. 9.

Finally, using the solutions of u_s, ε_s, and $-dp/dy$ given in Fig. 9, the contribution of various terms to the acceleration of particles in the spout can be further analyzed by employing conservation of the solid-phase momentum [46]:

$$\rho_p \frac{d\left[(1-\varepsilon_s)v_s^2\right]}{dy} = -(1-\varepsilon_s)\frac{dp}{dy} - \frac{d\sigma_s}{dy} - (1-\varepsilon_s) \times (\rho_p - \rho_f)g + \beta\left(u_s - v_s\right). \tag{19}$$

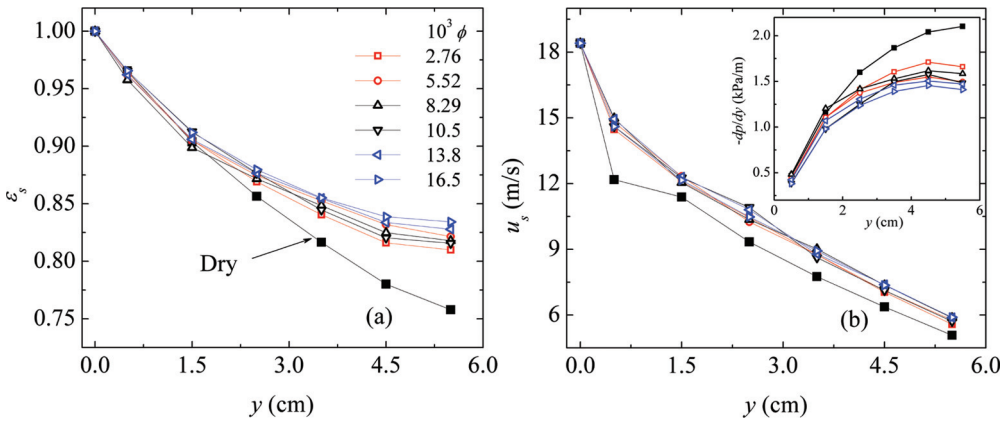

FIG. 9. (Color online) The longitudinal profiles of (a) voidages and (b) gas velocities along spout length for both dry and wet systems predicted by one-dimensional mass and momentum conservation model. Inset shows the profiles of pressure drop.

We estimate that a ratio of pressure drop to gravitational force, $(-dp/dy)/\rho_p g$, has a magnitude of 0.1 or much lower, implying that the pressure-gradient force is far too low to overcome the gravitation. Defining a terminal velocity u_t as $\sqrt{\frac{4}{3}(\rho_p/\rho_f - 1)gd_p/C_d}$, the dimensionless drag with respect to the gravitation is approximately given as $\varepsilon_s^{-1.65}(u_s - v_s)^2/u_t^2$ when $\varepsilon_s > 0.8$. In this work, Re_p ranges from 750 to 3000 based on the u_s given in Fig. 9, which ensures C_d in a narrow range of 0.44–0.48. Thus, the terminal u_t is at a magnitude of 10 m/s, causing a drag-gravitation ratio as large as 3 at the bottom of spout. Interestingly, when we ignore the solid stress term, $-d\sigma/dy$, the predicted $v_{p\max}$ $(=2v_s)$ by numerically integrating the first, third, and fourth terms on the right side of Eq. (19) well coincides with the measured PIV data, as shown in Fig. 7(c). The higher acceleration of wet grains can be mainly attributed to the larger drag instead of other terms, which originates from the higher voidage and higher gas velocity due to the reduction of spout width. This agreement indicates that the solid stress is almost vanishing in the dilute spout due to the limited particle-particle collisions and dissipations. For further detailed modeling, the existing granular continuum model starting from kinetic theory seems quite complex to the granular patterns in the spout, but also not accurate enough to capture quasistatic dense granular flows in the annulus. Nevertheless, the experimental findings in this work provide a good start for the development of discrete element model by incorporating the cohesion effect.

IV. SUMMARY

A quantitative comparison of the flow patterns of dry and wet granular materials in a 2DSB were conducted by using PIV. For both dry and wet grains, 2DSB possesses an intrinsic granular pattern, with the clustering granular gases in the dilute spout surrounded by the slow densely packed granular flows in the annulus. The effect of liquid cohesion on this complex granular pattern is multifold. First, it is observed that the presence of liquids with fraction (ϕ) ranging from 2.76 to 16.5×10^{-3} dramatically reduces the spout width, with the spout area of the wet cases being 84.2%–87.6% of those of the dry cases. Furthermore, for all wet cases, the upper part of the spout width is weakly dependent on ϕ, while the change of the lower part is inappreciable. Such distinct $r_s \sim \phi$ variation is one of those important macroscopic properties for testing discrete or continuum models of wet granular-fluid systems.

In the dense annulus, the cohesion enables wet grains to have a much lower downward velocity, v_y, than the dry ones. v_y slightly decreases with the increasing ϕ and approaches its minimum at 10.5×10^{-3}, corresponding to a maximum capillary force where the liquid bridge overcomes the particle roughness and reaches the spherical regime. Further increment of ϕ causes a small reincrement of v_y indicating the viscous lubrication effect. Meanwhile, in the dilute spout, we made the interesting discovery that the wet grains possess slightly smaller v_y than dry gains in the earlier $1/3$ of the spout (stage I), whereas they become dramatically larger in the rest $2/3$ of the spout (stage II). Starting from a unified lateral profile of v_y as a cubic function of x, a one-dimensional mass and momentum conservation model has been built and well interpreted the experimental data. Similar percolation from the spout to the annulus by the reduced spout area means a high gas velocity and voidage in the wet system, which results in the high acceleration of the wet grains in the spout. This finding in Fig. 7 could be helpful to the validation of the discrete element modeling in the future work.

ACKNOWLEDGMENTS

This work has been funded by the National Natural Science Funds of China (No. 50976058). We acknowledge Dr. Colin Thornton and Dr. Charley Wu at Birmingham for discussions at the UK-China Particle forum. S.Q.L. is grateful to Prof. Jeff Marshall at Vermont, Prof. Edward Law at Princeton and Dr. Guanqing Liu at Tsinghua for helpful discussions.

[1] S. Q. Li, J. S. Marshall, G. Q. Liu, and Q. Yao, Prog. Energy Combust. Sci. **37**, 63 (2011).
[2] J. M. Ottino and D. V. Khakhar, Annu. Rev. Fluid Mech. **32**, 55 (2000).
[3] G. Seiden and P. J. Thomas, Rev. Mod. Phys. **83**, 1323 (2011).
[4] I. S. Aranson and L. S. Tsimring, Rev. Mod. Phys. **78**, 614 (2006).
[5] H. M. Jaeger, S. R. Nagel, and R. P. Behringer, Rev. Mod. Phys. **68**, 1259 (1996).
[6] P. Jop, Y. Forterre, and O. Pouliquen, Nature (London) **441**, 727 (2006).
[7] C. R. Muller, D. J. Holland, A. J. Sederman, J. S. Dennis, and L. F. Gladden, Phys. Rev. E **82**, 050302 (2010).
[8] C. R. Muller, J. F. Davidson, J. S. Dennis, P. S. Fennell, L. F. Gladden, A. N. Hayhurst, M. D. Mantle, A. C. Rees, and A. J. Sederman, Phys. Rev. Lett. **96**, 154504 (2006).
[9] J. E. Fiscina, G. Lumay, F. Ludewig, and N. Vandewalle, Phys. Rev. Lett. **105**, 048001 (2010).
[10] Q. Xu, A. V. Orpe, and A. Kudrolli, Phys. Rev. E **76**, 031302 (2007).
[11] S. Herminghaus, Adv. Phys. **54**, 221 (2005).
[12] O. Pitois, P. Moucheront, and X. Chateau, J. Colloid Interface Sci. **231**, 26 (2000).
[13] C. D. Willett, M. J. Adams, S. A. Johnson, and J. P. K. Seville, Langmuir **16**, 9396 (2000).
[14] G. Lian, C. Thornton, and M. J. Adams, J. Colloid Interface Sci. **161**, 138 (1993).
[15] D. Hornbaker, R. Albert, I. Albert, A. L. Barabasi, and P. Schiffer, Nature (London) **387**, 765 (1997).
[16] R. Albert, I. Albert, D. Hornbaker, P. Schiffer, and A. L. Barabasi, Phys. Rev. E **56**, 6271 (1997).
[17] T. C. Halsey and A. J. Levine, Phys. Rev. Lett. **80**, 3141 (1998).

[18] T. G. Mason, A. J. Levine, D. Ertas, and T. C. Halsey, Phys. Rev. E **60**, 5044 (1999).
[19] A. V. Orpe and D. V. Khakhar, Phys. Rev. E **64**, 031302 (2001).
[20] H. M. Li and J. J. McCarthy, Phys. Rev. E **71**, 021305 (2005).
[21] S. Nowak, A. Samadani, and A. Kudrolli, Nat. Phys. **1**, 50 (2005).
[22] P. Tegzes, T. Vicsek, and P. Schiffer, Phys. Rev. E **67**, 051303 (2003).
[23] P. Tegzes, T. Vicsek, and P. Schiffer, Phys. Rev. Lett. **89**, 094301 (2002).
[24] R. Ojha, N. Menon, and D. J. Durian, Phys. Rev. E **62**, 4442 (2000).
[25] D. I. Goldman and H. L. Swinney, Phys. Rev. Lett. **96**, 145702 (2006).
[26] J. M. Valverde and A. Castellanos, Phys. Rev. E **75**, 031306 (2007).
[27] X.-L. Zhao, S. Q. Li, G. Q. Liu, Q. Yao, and J. S. Marshall, Powder Technol. **184**, 205 (2008).
[28] G. Q. Liu, S. Q. Li, X. L. Zhao, and Q. Yao, Chem. Eng. Sci. **63**, 1131 (2008).
[29] M. L. Passos and A. S. Mujumdar, Powder Technol. **110**, 222 (2000).
[30] N. A. Pohlman, J. M. Ottino, and R. M. Lueptow, Phys. Rev. E **80**, 031302 (2009).
[31] K. B. Mathur and N. Epstein, *Spouted Beds* (Academic Press, New York, 1974).
[32] R. K. Konduri, E. R. Altwicker, and M. H. Morgan III, Chem. Eng. Sci. **54**, 185 (1999).
[33] C. Vahlas, B. Caussat, P. Serp, and G. N. Angelopoulos, Mater. Sci. Eng. **53**, 1 (2006).
[34] O. M. Dogan, L. A. P. Freitas, C. J. Lim, J. R. Grace, and B. Luo, Chem. Eng. Commun. **181**, 225 (2000).
[35] L. A. P. Freitas, O. M. Dogan, C. J. Lim, J. R. Grace, and D. Bai, Can. J. Chem. Eng. **82**, 60 (2004).
[36] T. Schwager and T. Pöschel, Phy. Rev. E **78**, 051304 (2008).
[37] R. S. Krzywanski, N. Epstein, and B. D. Bowen, Chem. Eng. Sci. **44**, 1617 (1989).
[38] A. Yokogawa, E. Ogino, and N. Yoshii, Trans. Jpn. Soc. Mech. Eng. **38**, 148 (1972).
[39] S. Utermann, Ph.D. thesis, University of Göttingen, 2012.
[40] M. M. Kohonen, D. Geromichalos, M. Scheel, C. Schier, and S. Herminghaus, Physica A **339**, 7 (2004).
[41] C. L. Feng and A. B. Yu, Powder Technol. **99**, 22 (1998).
[42] G. A. Lefroy and J. F. Davidson, Trans. Inst. Chem. Eng. **47**, 120 (1969).
[43] M. H. Morgan, J. Y. Day, and H. Littman, Chem. Eng. Sci. **40**, 1367 (1985).
[44] R. Aguado, S. Alvarez, M. J. San Jose, M. Olazar, and J. Bilbao, in *15th European Symposium on Computer Aided Process Engineering, Spain*, edited by L. Puigjaner and A. Espuna (Elsevier Science B. V., 2005), p. 613.
[45] G. Rovero, C. M. H. Brereton, N. Epstein, J. R. Grace, L. Casalegno, and N. Piccinini, Can. J. Chem. Eng. **61**, 289 (1983).
[46] D. Gidaspow, *Multiphase Flow and Fluidization* (Academic Press, Boston, 1993), p. 42.